Dalton Transactions



PAPER View Article Online
View Journal | View Issue



Cite this: *Dalton Trans.*, 2021, **50**, 9648

Exploiting complementary ligands for the construction of square antiprismatic monometallic lanthanide SMMs†

Yushu Jiao, Da Sidra Sarwar, D‡a,b Sergio Sanz, D*‡b,c Jan van Leusen, Da Natalya V. Izarova, Da,b Cameron L. Campbell, Dd Euan K. Brechin, D*e Scott J. Dalgarno **D** and Paul Kögerler **D** **D**

Received 1st February 2021, Accepted 18th June 2021 DOI: 10.1039/d1dt00359c The methylation of p-tert-butylcalix[4]arene in the distal 1,3-phenolic sites provides the ligand $H_2L = \{p$ -tert-butylcalix[4](OMe)₂(OH)₂arene} that enables construction of heteroleptic mononuclear lanthanide complexes. The reaction of $(N(nBu)_4)(acac)$ (Hacac = acetylacetone), $M^{III}Cl_3$ and H_2L under Schlenk conditions results in the formation of a family of $(N(nBu)_4)[M^{III}L(acac)_2]$ complexes where M = Y (1), Gd (2), Tb (3) and Dy (4). The metal ions are eight-coordinate in distorted square-antiprismatic coordination geometries, resulting in slow relaxation of the magnetisation for the Tb derivative.

Introduction

The discovery of magnetic bi-stability and slow magnetisation relaxation processes of purely molecular origin in polymetallic Single-Molecule Magnets (SMMs)¹ three decades ago has evolved into a broader quest to understand and control the spin dynamics of coordination complexes comprising single, magnetically anisotropic spin centres (single-ion SMMs). In general, such systems exhibit an axial zero-field splitting of the m_J magnetic sublevels of the ground term^{2–5} and have been suggested for potential applications in quantum computation and molecular spintronics.^{6–13} In particular, the key discovery that the double-decker phthalocyanato-terbium(III) complex [TbPc₂]⁻ exhibits significant blocking of the magnetisation at the single Tb ion level $(U_{\rm eff} = 230~{\rm cm}^{-1})^{14}$ reinvigorated interest in the coordination chemistry of lanthanide ions. Primarily

this is due to the large intrinsic magnetic anisotropy originating from the near degeneracy of the 4f orbitals, but also from the ability to manipulate the magnitude and alignment of anisotropy axes through judicious ligand design. ^{15–21}

p-tert-Butylcalix[4]arene (TBC[4]) is a cone-shaped molecule comprising four phenolic units linked by methylene bridges.²² The upper-rim of TBC[4] increases solubility in organic solvents, whilst the polyphenolic lower-rim presents it as an ideal candidate for the complexation of paramagnetic transition (TM) and lanthanide (Ln) metal centres. This ligand has been employed to build a library of magnetic polynuclear complexes of TM, Ln and mixed TM-Ln metal ions, and has provided insight into how systematic modifications to the magnetic core and/or peripheral substituents affect the magnetic characteristics of these species. Although much of the exploration involves the formation of polynuclear clusters with transition metals, ^{23–29} the investigation on the binding modes of TBC[4] with reported Ln and mixed TM-Ln metal ions is paramount in the design of monometallic Ln-based systems (Fig. 1).

The synthesis of a series of TBC[4]-supported $\rm Ln_6^{III}$ clusters in 2012 represented the first example of a polynuclear lanthanide complex with this ligand. The general metallic core describes a $\rm [Ln_6^{III}]$ octahedron connected internally by two $\rm \mu_4$ - $\rm O^{2-}$ ions and sandwiched between two TBC[4] ligands (Fig. 1a). The magnetic behaviour of all family members did not reveal slow relaxation of the magnetisation above 1.8 K. A similar $\rm [Dy_6^{III}]$ structure was later reported with variations on the peripheral ligands, displaying slow relaxation of the magnetisation with a thermal energy barrier of 7.6 K. Several heterometallic complexes combining the properties of 3d–4f ions have also been investigated. These include clusters comprising

^aInstitute of Inorganic Chemistry, RWTH Aachen University, 52056 Aachen, Germany. E-mail: paul.koegerler@ac.rwth-aachen.de

^bPeter Grünberg Institute, Electronic Properties (PGI-6), Forschungszentrum Jülich, 52425 Jülich, Germany. E-mail: s.calvo@fz-juelich.de

⁶Jülich-Aachen Research Alliance, Fundamentals for Future Information Technology (JARA-FIT), Forschungszentrum Jülich, 52425 Jülich, Germany

^dInstitute of Chemical Sciences, Heriot-Watt University, Riccarton, Edinburgh, EH14 4AS, UK. E-mail: S.J.Dalgarno@hw.ac.uk

^eEaStCHEM School of Chemistry, The University of Edinburgh, David Brewster Road, Edinburgh, EH9 3FJ, UK. E-mail: ebrechin@ed.ac.uk

[†] Electronic supplementary information (ESI) available: Instrumentation; ESI-HRMS, UV-Vis, IR, TGA and PXRD data; magnetic studies and simulations; crystallographic analysis details. CCDC 2050769–2050772. For ESI and crystallographic data in CIF or other electronic format see DOI: 10.1039/d1dt00359c ‡ These authors contributed equally to this work.

Dalton Transactions Paper

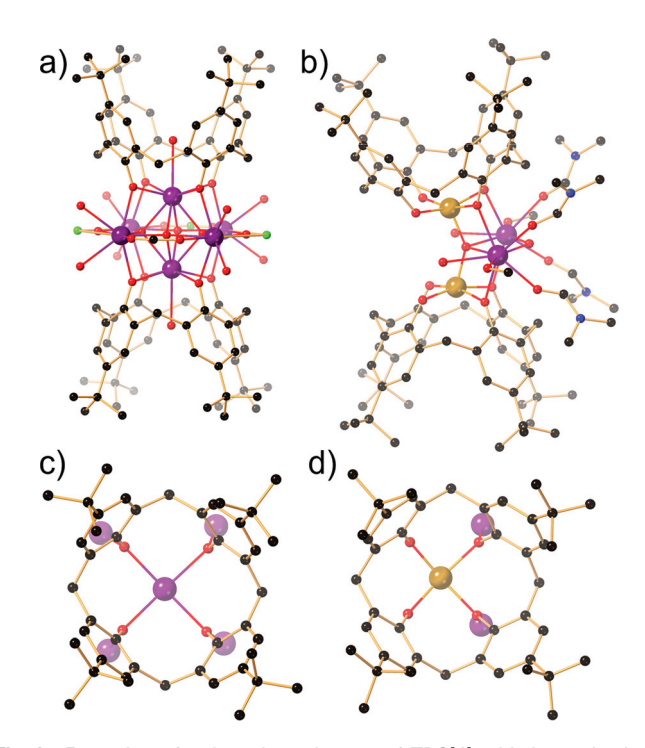


Fig. 1 Examples of polynuclear clusters of TBC[4] with Ln and mixed TM-Ln metal ions featuring (a) $[Tb_6^{III}(TBC[4])_2O_2(OH)_{3.32}Cl_{0.68}(HCO_2)_2$ $(dmf)_8(H_2O)_{0.5}]$ and (b) $[Fe_2^{|||}Tb_2^{|||}(O)(OH)(TBC[4])_2(dmf)_4(MeOH)_2(H_2O)_2]Cl$. Highlight of the TBC[4] binding modes, as top view, of the molecules depicted in (a) and (b): (c) [Tb₅^{|||}(TBC[4])] and (d) [Fe^{|||}Tb₂^{|||}(TBC[4])] motifs. Colour code: Tb = magenta, O = red, and C = black. H atoms and the Cl anion in (b) are omitted for clarity; terminal dmf molecules coordinated to the equatorial terbium atoms in (a) are represented only by the coordinating oxygen atom for clarity.

a [Mn₄^{III}Ln₄^{III}] core in which the central Ln₄ square is capped on each edge by four [Mn^{III}calix[4]arene] units. SMM behaviour was observed for the Tb^{III} and Dy^{III} derivatives, while the Gd^{III} analogue proved to be an excellent cryogenic refrigerant.³² TBC[4]-supported TM-Ln $[Mn_2^{III}Mn^{II}Ln^{III}]$ and $[Mn_2^{III}Ln_2^{III}]$ magnetic cores with butterfly topologies,³³ and a distorted [Fe₂^{III}Ln₂^{III}] tetrahedron (Fig. 1b).³⁴ In all Mn-Ln clusters the central Ln ions were sandwiched between two [Mn^{III}calix[4]arene] capping units.

The TBC[4] lower-rim houses TM or Ln metal ions in all of the aforementioned cases, and the oxygen atoms bridge to neighbouring metal centres within the resulting clusters. Although approaches such as variable stoichiometry offer some control in the assembly process (e.g. in the formation of [Mn₂^{III}Mn^{III}Ln^{III}] and [Mn₂^{III}Ln₂^{III}] butterflies),³³ precise control over the coordination sphere of a paramagnetic metal ion is both a worthwhile and timely pursuit. The constrained nature of the TBC[4] platform presents it as a perfect starting point to isolate a single paramagnetic metal ion in a highly axial symmetry, where the magnetic anisotropy of the Ln centre is known to be directly related to its ligand field symmetry.³⁵ This minimises quantum tunnelling of magnetisation (QTM) leading to a high energy barrier to magnetic relaxation (U_{eff}) and to a large blocking temperature (T_B) . ^{20,36–38} Despite this rational design, there is just one report of a mononuclear lanthanide-based SMM with TBC[4]; a seven-coordinate dysprosium ion encapsulated between a TBC[4] and a Kläui tripodal ligand. This complex displays field-induced (dc = 900 Oe) SMM behaviour with $U_{\rm eff}$ = 73.7 K and τ_0 = 9.1 × 10⁻⁹ s.³⁹ A small number of TBC[4]-based mononuclear lanthanide comhave also been constructed investigate luminescence.40-43 metal extraction 44,45 and synthetic methodology.46-51

In order to achieve high levels of control over the coordination sphere of a metal ion at the TBC[4] lower-rim, one must first overcome the preference for TBC[4] to bridge to neighbouring metal centres. A survey of the Cambridge Structural Database for TBC[4] bis-methylated at distal positions, p-tertbutylcalix[4](OMe)₂(OH)₂arene (referred to hereafter as H₂L) returned a complex of particular interest, [(p-tert-butylcalix[4] (OMe)₂(O)₂arene)Ce(acac)₂].⁵² Inspection of the structure reveals that the bulk of the lower-rim methyl groups, combined with that of the complementarity acac ligands directs the formation of a pseudo-square-antiprismatic ligand field for the Ln ion.

Inspired by this structure, we herein describe the synthesis and characterisation of a family of (N(nBu)₄)[M^{III}L(acac)₂] complexes where M = Y(1), Gd(2), Tb(3) and Dy(4) (Fig. 2), as well as a detailed analysis of the magnetic properties of 2-4.

Results and discussion

Complexes 1-4 were synthesised by reacting $(N(nBu)_4)(acac)$, M^{III}Cl₃ and H₂L (stoichiometry 4:1:1) in toluene at reflux for six hours under Schlenk conditions (see Experimental section). The resulting solution was filtered and the mother liquor evaporated to afford a yellow oil that was washed with CH₂Cl₂, yielding a pure product. Initially, we explored reaction conditions in the synthesis of (N(nBu)₄)[Y^{III}L(acac)₂] by ¹H NMR to access the more complicated paramagnetic analogues 2–4. The ¹H NMR (400 MHz, CD₃CN) spectrum of 1 in solution presents resonance signals characteristic of a C_{2v} symmetric structure, where two opposite aromatic rings are near-parallel

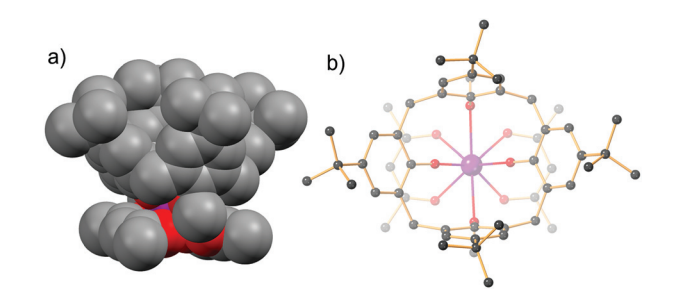


Fig. 2 (a) Space filling model of the molecular structure of the $[Y^{III}L]$ $(acac)_2$ anion in **1**. (b) Top view of the molecule highlighting the TBC[4] pinched conformation and coordination to a single metal ion. Colour code: Y = magenta, O = red, and C = black. H atoms are omitted for clarity.

Paper

and the other two tilted, characteristic of the pinched cone conformation of the ligand. Upon coordination, aromatic proton signals of the free ligand H2L present an upfield shift of \sim 0.30 ppm with singlets at 6.90 and 6.88 ppm (Fig. 3), while the diastereotopic methylene bridge protons also display upfield and downfield shifts upon complex formation. The axialprotons show a very small downfield shift of 0.13 ppm (to 4.40 ppm, CH_{2ax}), but the equatorial-protons are strongly affected by coordination to yttrium and display a large upfield shift of 0.53 ppm (2.87 ppm, CH_{2eq}). The methoxy groups also display a downfield shift of 0.14 ppm (4.10 ppm, CH₃O). Singlets (1.21 and 1.07 ppm, $CH_{3/Bu}$) corresponding to two different, symmetry unique, aromatic rings are almost unchanged (as expected) due to the distance of the tert-butyl groups to the metal centre. Integration of tetrabutylammonium signals is consistent with the presence of one cation.

Full characterisation of **1** by elemental analysis, IR, UV–Vis, ESI–HRMS and single-crystal X-ray crystallography (*vide infra*) support the assignments made *via* ¹H NMR; complexes **2–4** were subsequently synthesised and fully characterised by analogous techniques (see synthesis and characterisation of **1–4** in Experimental section).

Colourless rod-like single crystals of 1–4 were obtained by slow diffusion of CH₃CN into a concentrated THF solution of each complex. The crystals were all found to be of monoclinic symmetry, and structure solution was performed in the space group *Cc* (1 and 4) or *C2/c* (2 and 3) (Table S1†). The four complexes are structurally analogous; hence, we provide a representative description for 1 in the interest of brevity. The fully deprotonated calix[4]arene bonds the yttrium metal ion as a tetradentate ligand through the lower-rim O-atoms (Y^{III}–OPh: 2.149(6) and 2.150(5) Å; Y^{III}–OMePh: 2.593(5) and 2.611(6) Å), adopting a pinched-cone conformation where the two methylated aromatic rings pinch and the two phenoxide rings splay as shown in Fig. 2b and 4a. The "O₄" pocket presents as two triangular units (O2/O4/O3 and O2/O4/O1, Fig. 4a) linked at

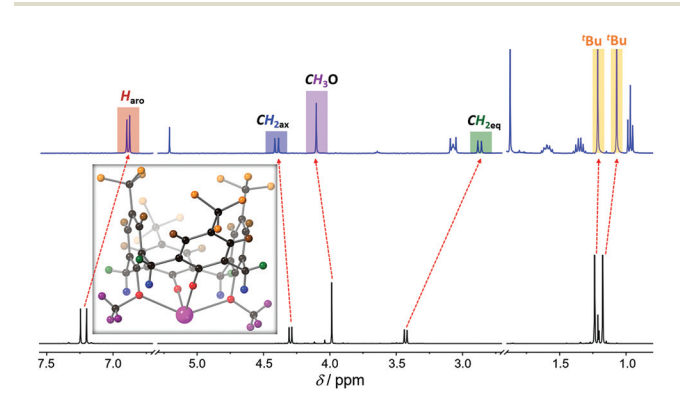


Fig. 3 1 H-NMR spectra (400 MHz, 300 K) in CD₃CN of (top) (N(nBu)₄) [Y^{III}L(acac)₂]; (bottom) H₂L = {p-tert-butylcalix[4](OMe)₂(OH)₂arene}. Representation of the different hydrogen atoms in the [Y^{III}((p-tert-butylcalix[4](OMe₂)O₂)]⁺ unit observable by 1 H NMR. Colour code: H-aromatics = red-brown, H-CH₂axial = blue, H-CH₃O = dark magenta, H-CH₂equatorial = green, and H- t butyl = orange.

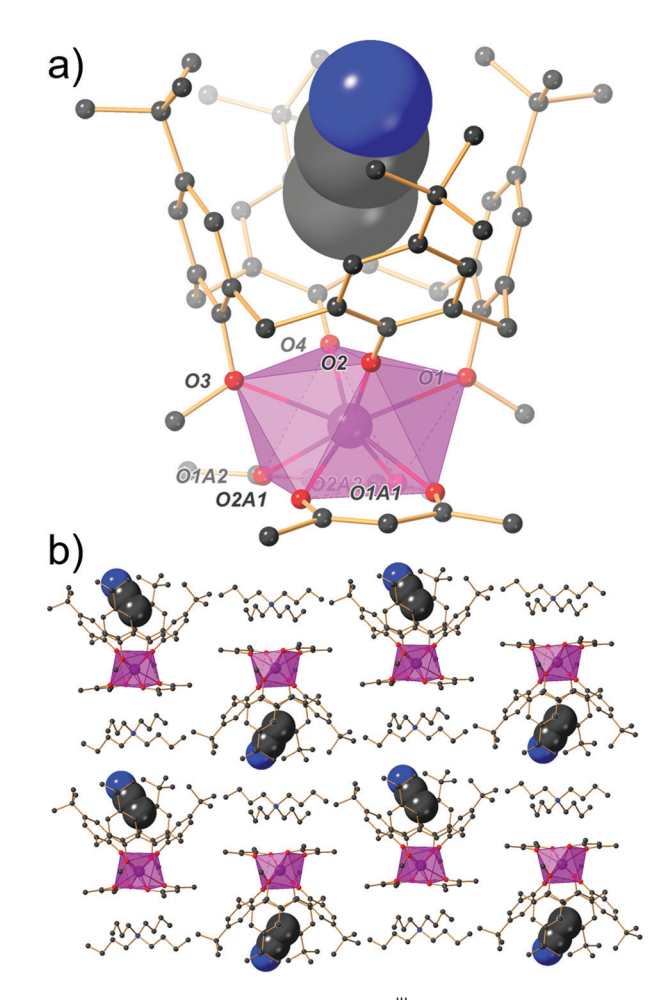


Fig. 4 (a) Molecular structure of the $[Y^{III}L(acac)_2]^-$ anion in 1, rotated 90° with respect to the space-filling representation in Fig. 2a. Highlighted in transparent magenta is the polyhedral representation of the coordination environment of the metal ion as a distorted square-antiprismatic $Y^{III}O_8$. (b) Extended structure of 1 showing the packing in an antiparallel bilayer array with molecules interdigitated, as seen for solvates of the naked TBC[4]. Molecules of CH_3CN are encapsulated in the TBC[4] cavities and, $(N(nBu)_4)^+$ countercations crystallise in the interstitial space. Colour code: Y = magenta, O = red, N = blue and C = black. H-atoms are omitted for clarity.

one " O_2 " edge (O2/O4) with a dihedral angle of 24.11°. The remaining coordination vacancies are occupied by two acac ligands (Y^{III}–O: 2.355(5)–2.387(6) Å) with the eight-coordinate Y^{III} centre adopting distorted square-antiprismatic geometry. Inspection of the structure of 1 in space-filling representation (Fig. 2a) clearly shows that bis-methylation, coupled with the use of acac as a complementary ligand, precludes bridging to other metal centres. The YO₈ fragment is rotated by a skew angle of 41.70–49.06° with respect to the eclipsed geometry, the molecule displaying a small distortion from C_{2v} symmetry, as indicated by NMR. Analysis of the extended structure shows that neighbouring molecules pack in an antiparallel bilayer array, akin to the solvates of the TBC[4], ^{53–55} with the inclusion of acetonitrile solvent molecules in the cavities (Fig. 4b), with N(nBu)₄ cations providing charge balance in the interstitial

spaces. This arrangement isolates the magnetic unit from neighbouring symmetry equivalents, with the closest contacts mediated by $CH_3(\text{ketone})$ –CH(Ph) and $CH_3(^t\text{Bu})$ – $CH_3(\text{OMePh})$ interactions at 3.692 and 3.625 Å, respectively. The shortest Y^{III} – Y^{III} distance is 11.217 Å. There are no intra- or intermolecular hydrogen bonds, and the closest intermolecular distance to $N(n\text{Bu})_4$ is 3.218 Å (O(ketone)– $CH_2(N(n\text{Bu})_4)$.

Dalton Transactions

The electronic absorption spectra of 1-4 in CH₂Cl₂ present two peaks with λ_{max} at ~270 and 281 nm, attributed to a $(\pi - \pi^*)$ transition centred on the phenyl rings of the TBC[4] ligand and β-diketonates (Fig. S3,† left). FT-IR spectra display vibrations associated with ν (C-H) ~2960-2850 cm⁻¹ (s), ν (C- $O_{delocalised}$)_{acac} ~1597 cm⁻¹ (s), ν (C- $C_{delocalised}$)_{acac} ~1508 cm⁻¹ (s), overlapping vibrations of $\nu(arC-C)/\delta(CH_2)/\delta_{as}(CH_3)$ $\sim 1481-1410$ cm⁻¹ (vs), δ_s (CH₃) ~ 1332 cm⁻¹ (m), ν (C-O) ~1210 cm⁻¹ (w) and γ (CH₃) ~1007 cm⁻¹ (m) (Fig. S3,† right). ESI-HRMS in the negative ion mode shows the presence of one main ion, the singly charged $[M - N(nBu)_4]^-$ (M = $(N(nBu)_4)[M^{III}L(acac)_2]$, with 100% relative abundance for M = Y, Gd, Dy and, 30% for M = Tb (Fig. S1 and S2†). The isotopic distributions of the calculated species show m/z deviations within 0.001 of the found ionic values. Elemental analysis of 1-4 agrees with the empirical formula $C_{74}H_{111}N_2O_8M$ (M = Y, Gd, Tb and Dy) with a deviation within 0.3% (absolute; see Experimental section). Thermogravimetric analysis (TGA) shows the stability of complexes 1-4 up to ca. 160 °C corresponding with the gradual loss of crystallised CH₃CN molecules (Fig. S4†).

Direct current (dc) magnetic susceptibility and magnetisation measurements for 2-4 are shown as $\chi_{\rm m}T$ vs. T at 0.1 and 1.0 T and $M_{\rm m}$ vs. B at 2.0 K and B = 0.1–5.0 T. At 290 K, the $\chi_{\rm m}T$ values of 7.84 (2), 11.90 (3) and 13.79 cm³ K mol⁻¹ (4) are within the ranges expected for the respective isolated Ln^{III} centres: 56 7.6–7.9 (2, Gd $^{\rm III}$), 11.7–12.0 (3, Tb $^{\rm III}$) and 13.0–14.1 cm³ K mol⁻¹ (4, Dy^{III}). $\chi_{\rm m}T$ values (2 and 3) gradually decrease to 7.60 cm³ K mol⁻¹ (2) and 10.92 cm³ K mol⁻¹ (3) minima at 4.5 K, exhibiting a small upturn to 7.76 cm³ K mol⁻¹ (2) and 11.13 cm³ K mol⁻¹ (3) at 2.0 K. Complex 4 displays a progressive decrease in the $\chi_{\rm m}T$ value to 12.82 cm³ K mol⁻¹ at 25.0 K, wherefrom it drops to 10.92 cm³ K mol⁻¹ at 2.0 K. Since Gd^{III} has an almost isotropic S = 7/2 (${}^8S_{7/2}$), the Curie-like temperature invariant $\chi_m T$ value is readily explained. For 3 and 4, the decrease of $\chi_m T$ at T < 150 K is due to the thermal depopulation of the m_I energy sublevels of the ground multiplets (which are essentially 7F_6 for Tb^{III} and ${}^6H_{15/2}$ for DyIII) substantially split by spin-orbit coupling, interelectronic repulsion and ligand field effects. The observation of a small upturn for 2 and 3 at low temperature, likely indicates the presence of very weak, intermolecular ferromagnetic dipolar exchange interactions. At T > 20 K, the shape of the $\chi_{\rm m} T$ vs. Tcurves (2-4) are similar to those observed with B = 1.0 T, below which they distinctly drop off due to the significant saturation effects caused by the Zeeman contributions at such fields (Fig. 5a). At 2 K, the molar magnetisation $M_{\rm m}$ vs. applied field B (Fig. 5a, inset) of 2-4 show an approximately linear dependence at B < 0.5 T and saturation effects at higher fields; the

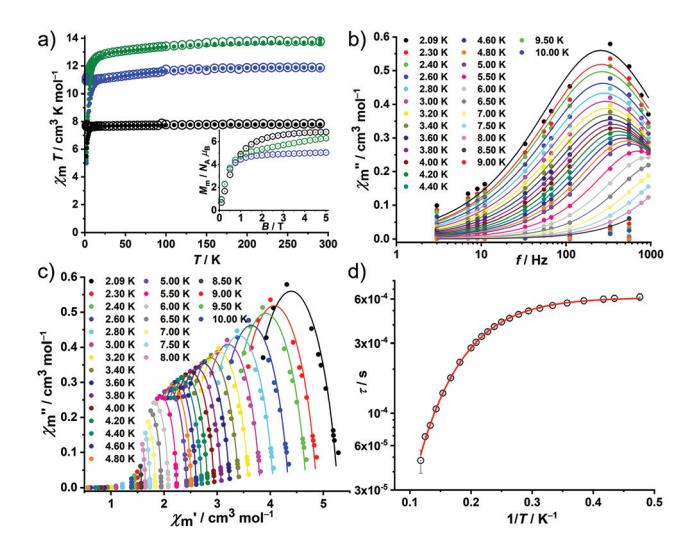


Fig. 5 (a) Dc data: $\chi_m T$ vs. T at 0.1 (empty circles) and 1 T (filled circles) and, $M_{\rm m}$ vs. B at 2.0 K (inset) for 2 (black circles), 3 (blue circles) and 4 (green circles). (b) Out-of-phase molar magnetic susceptibility $\chi''_{\rm m}$ vs. f for 3 (filled circles: data, lines: fits to generalised Debye expression). (c) Magnetic ac data for 3: Cole–Cole plot in the range 2.09–10.0 K at a static bias field of 300 Oe (filled circles: data, lines: fits to a generalised Debye expression). (d) Plot of relaxation time τ vs. T^{-1} (empty circles at 2.09 K $\leq T \leq$ 8.5 K) for 3; the solid red line shows a combined fit considering quantum tunnelling of magnetisation and Raman slow relaxation processes.

values of $M_{\rm m}$ at 5.0 T are 6.9 (2), 5.0 (3) and 6.3 $N_{\rm A}\mu_{\rm B}$ (4). While the (almost) isotropic Gd^{III} centre in 2 is close to saturation ($M_{\rm m,sat}$ = 7.0 $N_{\rm A}\mu_{\rm B}$) at 5.0 T and 2.0 K, the anisotropic centres in 3 (Tb^{III}) and 4 (Dy^{III}) reach roughly 60% of their saturation magnetisations (9.0 and 10.0 $N_{\rm A}\mu_{\rm B}$, respectively). This is due to the measurement of powdered samples, *i.e.* the determination of the mean value of randomly oriented crystallites consisting of magnetically anisotropic centres. Thus, the magnetisation data at 2.0 K of all complexes agree with the absence or presence of very weak ferromagnetic intermolecular exchange interactions.

For 2 marginal out-of-phase signals (χ''_m) at zero static bias field were detected (Fig. S6c†). For 4, the application of various static bias fields up to 1000 Oe were necessary to obtain curvature in the Cole-Cole plot of the out-of-phase (χ''_m) vs. the inphase magnetic susceptibility ($\chi'_{\rm m}$) data (Fig. S7a†). Since these signals are not well defined, we focus on the ac data analysis of 3 (see the ESI for more details for 2 and 4). At zero static bias field, no out-of-phase signals were detected for complex 3; scanning the static magnetic field revealed optimal signals at 300 Oe (Fig. 5b and c). Simultaneously fitting a generalised Debye expression⁵⁷ to the $\chi'_{\rm m}$ vs. f and $\chi''_{\rm m}$ vs. f data, yields the solid lines shown in Fig. 5b and c and the relaxation times τ shown in Fig. 5d. The distribution of the relaxation times, α , suggests several relaxation pathways ($\alpha = 0.157 \pm$ 0.091). We found the best reproduction of the τ vs. 1/T data required considering a field independent contribution of the quantum tunnelling of magnetisation (QTM) and a Raman relaxation process, as combined in the formula $\tau^{-1} = B + CT^n$.

Paper Dalton Transactions

The best fit yields the constant $B = (1.58 \pm 0.02) \times 10^3 \text{ s}^{-1}$ for the QTM, and a constant $C = (3.06 \pm 0.17) \text{ s}^{-1} \text{ K}^{-n}$ and an exponent $n = 4.03 \pm 0.03$ for the Raman process. These parameters indicate either a Raman process based on the interaction between the spin and two photons for very widely spaced energy levels, or, considering the non-Kramers nature of TbIII, a process based on the combination of an optical and an acoustic phonon absorption/emission in the spin transition process.58

Conclusions

We report the synthesis and characterisation of a family of mononuclear complexes $(N(nBu)_4)[M^{III}L(acac)_2]$ by combining two complementary O-donor ligands, acac and p-tert-butylcalix [4] arene bis-methyl ether, which isolate Ln metal ions as eightcoordinate in a distorted square-antiprismatic coordination geometry. The Tb complex (3) shows typical SMM behaviour, whose relaxation of the magnetisation has been analysed considering both QTM and Raman processes. The Gd (2) and Dy (4) derivatives exhibit very weak out-of-phase ac susceptibility components, which we attribute to the structural distortion of the O_8 environment that in these compounds is only C_{2v} -symmetric, deviating from the D_{4d} -symmetric ideal. In a previous study,⁵⁹ we showed how a monolacunary polyoxometalate can act as a perfect tetradentate ligand to achieve mononuclear lanthanide complexes when combined with phthalocyanine ligands. Therefore, it may also be the case that the complexes reported here may act as ideal starting materials for the construction of hybrid calix[4]arene-polyoxometalate lanthanide double-deckers. These studies are currently underway, with a view to monitoring acac ligand metathesis reaction with monolacunary Keggin and Wells-Dawson polyoxometalates. Results from this work will be reported in due course.

Experimental section

Reagents were used as received from commercial suppliers. High-grade solvents were obtained from a MBRAUN MB-SPS 800 solvent purification system.

Synthesis of $(N(nBu)_4)[M^{III}L(acac)_2]$

A solution of acetylacetone (0.20 mL, 2 mmol) and $(N(nBu)_4)$ OH (1.30 mL from a 40 wt% in MeOH, 2 mmol) in 40 mL of methanol was stirred for two hours at 60 °C. The reaction mixture was then evaporated under reduced pressure to obtain a yellow oil featuring (N(nBu)4)(acac). To this residue, dry M^{III}Cl₃ (0.5 mmol), H₂L (338.49 mg, 0.5 mmol) and 50 mL of toluene was added under Ar and stirred at 135 °C for six hours. The solution was cooled, filtered and evaporated to dryness, before washing with dichloromethane to obtain a white powder. Colourless, block/rod X-ray quality crystals were obtained from a tetrahydrofuran solution of the product layered with acetonitrile. Yield (257 mg, 41% for 1); (265 mg,

40% for 2); (270 mg, 41% for 3) and (270 mg, 41% for 4). It should be noted that, whilst isostructural, the single crystal X-ray structures of 1/4 and 2/3 were solved in the space groups Cc and C2/c, respectively. It was possible to solve 1-4 in the latter, but in the case of 1 and 4 this caused significant disorder issues and poor refinement.

Analytical characterisation of 1-4

 $(N(nBu)_4)[Y^{III}L(acac)_2]$ (1). ¹H NMR (400 MHz, CD₃CN): δ 6.90 (s, 4H, ArH), 6.88 (s, 4H, ArH), 5.21 (s, 2H, acac-CH), 4.40 $(d, J = 11.3 \text{ Hz}, 4H, CH_{2ax}), 4.10 \text{ (s, 6H, OC}H_3), 3.09-3.06 \text{ (m, }$ 8H, $N(nBu)_4$ -NC H_2), 2.87 (d, J = 11.3 Hz, 4H, CH_{2eq}), 1.87 (s, 12H, acac- CH_3), 1.62-1.57 (m, 8H, $N(nBu)_4$ - NCH_2CH_2), 1.38–1.32 (m, 8H, $N(nBu)_4$ – $N(CH_2)_2CH_2$), 1.21 (s, 18H, ^tBu– CH_3), 1.07 (s, 18H, ${}^tBu-CH_3$), 0.97 (t, J = 7.3 Hz, 12H, $N(nBu)_4 N(CH_2)_3CH_3$) ppm.

ESI-HRMS m/z: found 961.42963 [M - N(nBu)₄]⁻ (100%) relative abundance), calculated for [C₅₆H₇₂O₈Y]⁻ 961.4291. M stands for $(N(nBu)_4)[Y^{III}L(acac)_2]$. Elemental analysis (%) calculated for $(C_{74}H_{111}N_2O_8Y)$ $\{(N(nBu)_4)[Y^{III}L(acac)_2]\cdot CH_3CN\}$: C, 71.36; H, 8.98; N, 2.25. Found C, 71.48; H, 8.89; N, 2.27. IR (KBr pellet, ν/cm^{-1}): 2965 (s), 2898(m), 2875(m), 1599(s), 1512(s), 1481(vs), 1411(m), 1334(m), 1254(w), 1212(w), 1170(w), 1124(w), 1095(w), 1007(m), 911(w), 871(w), 838(w), 792(w), 753(w), 717(w), 654 (w), 526(w), 494(w).

UV-Vis, THF solution, $\lambda/\text{nm} \ (\epsilon/10^4 \text{ M}^{-1} \text{ cm}^{-1})$: 269.8 (3.25), 279.2 (3.31). Crystal data for 1 (CCDC 2050769†): $C_{74}H_{111}N_2O_8Y$, $M_r = 1245.5 \text{ g mol}^{-1}$, colourless block, 0.09 × $0.19 \times 0.30 \text{ mm}^3$, monoclinic, space group Cc, a = 23.819(5) Å, $b = 16.065(3), c = 21.035(4) \text{ Å}, \beta = 120.38^{\circ}, V = 6945(3) \text{ Å}^3, Z = 4$ STOE STADIVARI diffractometer, MoK α radiation (λ = 0.71073 Å), T = 100(15) K, 41 717 reflections collected, 12 916 unique ($R_{\text{int}} = 0.0640$), 10 286 observed ($I > 2\sigma(I)$). Final GooF = 1.036, $R_1 = 0.0652$ ($I > 2\sigma(I)$) and w $R_2 = 0.1588$ (all data).

 $(N(nBu)_4)[Gd^{III}L(acac)_2]$ (2). ESI-HRMS found $1030.44564 [M - N(nBu)_4]^-$ (100% relative abundance), calculated for $[C_{56}H_{72}O_8Gd]^-$ 1030.4474. M stands for $(N(nBu)_4)$ [Gd^{III}L(acac)₂]. Elemental analysis (%) calculated for $(C_{74}H_{111}N_2O_8Gd)$ { $(N(nBu)_4)[Gd^{III}L(acac)_2]\cdot CH_3CN$ }: C, 67.64; H, 8.52; N, 2.13. Found C, 67.63; H, 8.50; N, 2.07. IR (KBr pellet, n/cm^{-1}): 2961(s), 2901(m), 2874(m), 1595(s), 1509(s), 1482(vs), 1410(m), 1332 (m), 1252(m), 1209(w), 1170(w), 1123(w), 1092(w), 1005(w), 911(w), 866(m), 839(w), 792(w), 755(w), 718(w), 654(w), 527(w), 497(w). **UV-Vis**, THF solution, λ / nm ($\varepsilon/10^4$ M⁻¹ cm⁻¹): 270.5 (2.84) and 281.3 (2.96). Crystal data (CCDC 2050770†): $C_{74}H_{111}N_2O_8Gd$, $M_r = 1313.89 \text{ g mol}^{-1}$, colourless block, $0.20 \times 0.26 \times 0.42 \text{ mm}^3$, monoclinic, space group C2/c, a = 23.8101(7) Å, b = 16.0920(5), c = 21.0561(10) Å, $\beta = 120.3280(10)^{\circ}$, $V = 6963.6(4) \text{ Å}^3$, Z = 4, Bruker D8 Venture diffractometer, MoK α radiation ($\lambda = 0.71073$ Å), T = 100 K, 101 381 reflections collected, 7678 unique ($R_{\text{int}} = 0.0589$), 6767 observed $(I > 2\sigma(I))$. Final GooF = 1.363, $R_1 = 0.0442 \ (I > 2\sigma(I))$ and $wR_2 = 0.1122$ (all data).

 $(N(nBu)_4)[Tb^{III}L(acac)_2]$ (3). **ESI-HRMS** m/z: found $1031.44670 [M - N(nBu)_4]^-$ (29.86% relative abundance), calculated for $[C_{56}H_{72}O_8Tb]^-$ 1031.4475. M stands for $(N(nBu)_4)$ [Tb^{III}L(acac)₂]. Elemental analysis (%) calculated for $(C_{74}H_{111}N_2O_8Tb) \{(N(nBu)_4)[Tb^{III}L(acac)_2]\cdot CH_3CN\}: C, 67.56; H,$ 8.50; N, 2.13. Found C, 67.26; H, 8.44; N, 2.05. IR (KBr pellet, ν/cm^{-1}): 2963(s), 2899(m), 2874(m), 1595(s), 1509(s), 1480(vs), 1411(s), 1334(s), 1253(w), 1210(w), 1170(w), 1124(w), 1095(w), 1007(m), 910(w), 871(w), 839(w), 792(w), 756(w), 719(w), 651(w), 528(w), 496(w). UV-Vis, THF solution, λ/nm ($\varepsilon/10^4 \text{ M}^{-1}$ cm⁻¹): 269.8 (2.99) and 281.3 (3.01). Crystal data (CCDC **2050771**†): $C_{74}H_{111}N_2O_8Tb$, $M_r = 1315.56$ g mol⁻¹, colourless rod, $0.24 \times 0.26 \times 0.46$ mm³, monoclinic, space group C2/c, a =23.8191(5) Å, b = 16.0761(4), c = 21.0672(5) Å, $\beta = 120.3400$ $(10)^{\circ}$, V = 6962.2(3) Å³, Z = 4, Bruker D8 Venture diffractometer, CuK α radiation ($\lambda = 1.54178 \text{ Å}$), T = 100(2) K, 143 474 reflections collected, 7092 unique ($R_{int} = 0.0381$), 7005 observed (I > $2\sigma(I)$). Final GooF = 1.387, $R_1 = 0.0526 \ (I > 2\sigma(I))$ and $wR_2 =$ 0.1399 (all data).

(N(nBu)₄)[Dy^{III}L(acac)₂] (4). ESI-HRMS m/z: found 1036.45154 [M – N(nBu)₄]⁻ (100% relative abundance), calculated for [C₅₆H₇₂O₈Dy]⁻ 1036.4513. M stands for (N(nBu)₄) [Dy^{III}L(acac)₂]. Elemental analysis (%) calculated for (C₇₄H₁₁₁N₂O₈Dy) {(N(nBu)₄)[Dy^{III}L(acac)₂]·CH₃CN}: C, 67.37; H, 8.48; N, 2.12. Found C, 67.60; H, 8.60; N, 2.09. IR (KBr pellet, ν /cm⁻¹): 2961(s), 2899(m), 2874(m), 1596(s), 1510(s), 1481(vs), 1429(m), 1411(s), 1382(m), 1346(m), 1334(s), 1311(w), 1253(w), 1210(w), 1170(w), 1124(w), 1095(w), 1007(m), 910(w), 871(w), 839(w), 792(w), 756(w), 718(w), 653(w), 528(w), 496(w). UV-Vis, THF solution, λ /nm (ε /10⁴ M⁻¹ cm⁻¹): 270.5 (2.80) and 281.9 (2.84).

Crystal data (CCDC 2050772†)

 $C_{74}H_{111}N_2O_8Dy$, $M_r = 1319.14$ g mol⁻¹, colourless rod, 0.20 × 0.26 × 0.40 mm³, monoclinic, space group Cc, a = 23.8297(6) Å, b = 16.0808(4), c = 21.0550(5) Å, $\beta = 120.3390(10)^\circ$, V = 6963.3 (3) Å³, Z = 4, Bruker D8 Venture diffractometer, MoKα radiation ($\lambda = 0.71073$ Å), T = 100(2) K, 95 871 reflections collected, 15 176 unique ($R_{\rm int} = 0.0177$), 14 735 observed ($I > 2\sigma(I)$). Final GooF = 1.038, $R_1 = 0.0144$ ($I > 2\sigma(I)$) and $wR_2 = 0.0393$ (all data).

Conflicts of interest

There are no conflicts to declare.

Acknowledgements

We thank the Chinese Scholarship Council (CSC) and the Punjab Educational Endowment Fund (PEEF) for Ms Yushu Jiao and Sidra Sarwar scholarships. EKB thanks the EPSRC (EP/N01331X/1).

Notes and references

1 A. Caneschi, D. Gatteschi, R. Sessoli, A. L. Barra, L. C. Brunei and M. Guillot, *J. Am. Chem. Soc.*, 1991, 113, 5873–5874.

- 2 M. A. Novak, R. Sessoli, D. Gatteschi and A. Caneschi, *Nature*, 1993, 365, 141–143.
- 3 G. Christou, D. Gatteschi, D. N. Hendrickson and R. Sessoli, *MRS Bull.*, 2000, 25, 66–71.
- 4 C. J. Milios and R. E. P. Winpenny, *Struct. Bonding*, 2015, **164**, 1–110.
- 5 J. M. Frost, K. L. M. Harriman and M. Murugesu, *Chem. Sci.*, 2016, 7, 2470–2491.
- 6 L. Bogani and W. Wernsdorfer, *Nat. Mater.*, 2008, 7, 179-
- 7 S. Thiele, F. Balestro, R. Ballou, S. Klyatskaya, M. Ruben and W. Wernsdorfer, *Science*, 2014, 344, 1135–1138.
- 8 A. Cornia, M. Mannini, P. Sainctavit and R. Sessoli, *Chem. Soc. Rev.*, 2011, **40**, 3076–3091.
- 9 G. Aromí, D. Aguilà, P. Gamez, F. Luis and O. Roubeau, *Chem. Soc. Rev.*, 2012, 41, 537–546.
- 10 E. Moreno-Pineda, C. Godfrin, F. Balestro, W. Wernsdorfer and M. Ruben, *Chem. Soc. Rev.*, 2018, 47, 501–513.
- 11 A. Gaita-Ariño, F. Luis, S. Hill and E. Coronado, *Nat. Chem.*, 2019, 11, 301–309.
- 12 A. Ghirri, A. Candini and M. Affronte, *Magnetochemistry*, 2017, 3, 12.
- 13 M. Urdampilleta, N. V. Nguyen, J. P. Cleuziou, S. Klyatskaya, M. Ruben and W. Wernsdorfer, *Int. J. Mol. Sci.*, 2011, **12**, 6656–6667.
- 14 N. Ishikawa, M. Sugita, T. Ishikawa, S. Y. Koshihara and Y. Kaizu, *J. Am. Chem. Soc.*, 2003, **125**, 8694–8695.
- 15 N. Ishikawa, M. Sugita, T. Okubo, N. Tanaka, T. Iino and Y. Kaizu, *Inorg. Chem.*, 2003, **42**, 2440–2446.
- 16 N. Ishikawa, M. Sugita, N. Tanaka, T. Ishikawa, S. Y. Koshihara and Y. Kaizu, *Inorg. Chem.*, 2004, 43, 5498– 5500.
- 17 M. Gonidec, F. Luis, A. Vílchez, J. Esquena, D. B. Amabilino and J. Veciana, *Angew. Chem., Int. Ed.*, 2010, 49, 1623–1626.
- 18 N. Ishikawa, M. Sugita, T. Ishikawa, S. Y. Koshihara and Y. Kaizu, *J. Phys. Chem. B*, 2004, **108**, 11265–11271.
- 19 S. Da Jiang, B. W. Wang, H. L. Sun, Z. M. Wang and S. Gao, J. Am. Chem. Soc., 2011, 133, 4730–4733.
- 20 L. Ungur, J. J. Leroy, I. Korobkov, M. Murugesu and L. F. Chibotaru, *Angew. Chem., Int. Ed.*, 2014, 53, 4413–4417.
- 21 S. Da Jiang, B. W. Wang, G. Su, Z. M. Wang and S. Gao, Angew. Chem., Int. Ed., 2010, 49, 7448–7451.
- 22 C. D. Gutsche, *Calixarenes 2001*, Kluwer Academic Publishers, 2001.
- 23 S. M. Taylor, J. M. Frost, R. McLellan, R. D. McIntosh, E. K. Brechin and S. J. Dalgarno, *CrystEngComm*, 2014, 16, 8098–8101.
- 24 S. M. Taylor, G. Karotsis, R. D. McIntosh, S. Kennedy, S. J. Teat, C. M. Beavers, W. Wernsdorfer, S. Piligkos, S. J. Dalgarno and E. K. Brechin, *Chem. – Eur. J.*, 2011, 17, 7521–7530.
- 25 S. M. Taylor, R. D. McIntosh, C. M. Beavers, S. J. Teat, S. Piligkos, S. J. Dalgarno and E. K. Brechin, *Chem. Commun.*, 2011, 47, 1440–1442.

Paper **Dalton Transactions**

- 26 G. Karotsis, S. J. Teat, W. Wernsdorfer, S. Piligkos, S. J. Dalgarno and E. K. Brechin, Angew. Chem., Int. Ed., 2009, 48, 8285-8288.
- 27 M. Coletta, S. Sanz, E. K. Brechin and S. J. Dalgarno, Dalton Trans., 2020, 49, 9882-9887.
- 28 M. Coletta, S. Sanz, L. J. McCormick, S. J. Teat, E. K. Brechin and S. J. Dalgarno, Dalton Trans., 2017, 46, 16807-16811.
- 29 R. McLellan, M. A. Palacios, S. Sanz, E. K. Brechin and S. J. Dalgarno, Inorg. Chem., 2017, 56, 10044-10053.
- 30 S. Sanz, R. D. Mc Intosh, C. M. Beavers, S. J. Teat, M. Evangelisti, E. K. Brechin and S. J. Dalgarno, Chem. Commun., 2012, 48, 1449-1451.
- 31 Y. Bi, G. Xu, W. Liao, S. Du, R. Deng and B. Wang, Sci. China: Chem., 2012, 55, 967-972.
- 32 G. Karotsis, S. Kennedy, S. J. Teat, C. M. Beavers, D. A. Fowler, J. J. Morales, M. Evangelisti, S. J. Dalgarno and E. K. Brechin, J. Am. Chem. Soc., 2010, 132, 12983-12990.
- 33 M. A. Palacios, R. McLellan, C. M. Beavers, S. J. Teat, H. Weihe, S. Piligkos, S. J. Dalgarno and E. K. Brechin, Chem. - Eur. J., 2015, 21, 11212-11218.
- 34 S. Sanz, K. Ferreira, R. D. McIntosh, S. J. Dalgarno and E. K. Brechin, Chem. Commun., 2011, 47, 9042-9044.
- 35 J. L. Liu, Y. C. Chen and M. L. Tong, Chem. Soc. Rev., 2018, 47, 2431-2453.
- 36 C. R. Ganivet, B. Ballesteros, G. De La Torre, J. M. Clemente-Juan, E. Coronado and T. Torres, Chem. -Eur. J., 2013, 19, 1457-1465.
- 37 Y. C. Chen, J. L. Liu, L. Ungur, J. Liu, Q. W. Li, L. F. Wang, Z. P. Ni, L. F. Chibotaru, X. M. Chen and M. L. Tong, J. Am. Chem. Soc., 2016, 138, 2829-2837.
- 38 J. Wu, O. Cador, X. L. Li, L. Zhao, B. Le Guennic and J. Tang, Inorg. Chem., 2017, 56, 11211-11219.
- 39 F. Gao, L. Cui, Y. Song, Y. Z. Li and J. L. Zuo, Inorg. Chem., 2013, 53, 562-567.
- 40 C. R. Driscoll, B. L. Reid, M. J. McIldowie, S. Muzzioli, G. L. Nealon, B. W. Skelton, S. Stagni, D. H. Brown, M. Massi and M. I. Ogden, Chem. Commun., 2011, 47, 3876-3878.

- 41 D. D'Alessio, S. Muzzioli, B. W. Skelton, S. Stagni, M. Massi and M. I. Ogden, Dalton Trans., 2012, 41, 4736-4739.
- 42 R. S. Viana, C. A. F. Oliveira, J. Chojnacki, B. S. Barros, S. Alves-Jr and J. Kulesza, J. Solid State Chem., 2017, 251, 26-32.
- 43 C. R. Driscoll, B. W. Skelton, M. Massi and M. I. Ogden, Supramol. Chem., 2016, 28, 567-574.
- 44 P. D. Beer, M. G. B. Drew, A. Grieve, M. Kan, P. B. Leeson, G. Nicholson, M. I. Ogden and G. Williams, Chem. Commun., 1996, 1, 1117-1118.
- 45 P. D. Beer, M. G. B. Drew, M. Kan, P. B. Leeson, M. I. Ogden and G. Williams, Inorg. Chem., 1996, 35, 2202-2211
- 46 G. L. Nealon, M. Mocerino, M. I. Ogden and B. W. Skelton, J. Inclusion Phenom. Macrocyclic Chem., 2009, 65, 25-30.
- 47 P. D. Beer, M. G. B. Drew, P. B. Leeson and M. I. Ogden, Inorg. Chim. Acta, 1996, 246, 133-141.
- 48 F. Estler, E. Herdtweck and R. Anwander, J. Chem. Soc., Dalton Trans., 2002, 65, 3088-3089.
- 49 J. Gottfriedsen, R. Hagner, M. Spoida and Y. Suchorski, Eur. J. Inorg. Chem., 2007, 2288-2295.
- 50 M. J. McIldowie, B. W. Skelton, M. Mocerino and M. I. Ogden, J. Inclusion Phenom. Macrocyclic Chem., 2015, 82, 43-46.
- 51 M. I. Ogden, B. W. Skelton and A. H. White, C. R. Chim., 2005, 8, 181-187.
- 52 J. Gottfriedsen and D. Dorokhin, Z. Anorg. Allg. Chem., 2005, 631, 2928-2930.
- 53 J. L. Atwood, L. J. Barbour, A. Jerga and B. L. Schottel, Science, 2002, 298, 1000-1002.
- 54 E. B. Brouwer, G. D. Enright and J. A. Ripmeester, J. Am. Chem. Soc., 1997, 119, 5404-5412.
- 55 G. D. Andreetti, R. Ungaro and A. Pochini, J. Chem. Soc., Chem. Commun., 1979, 1005-1007.
- 56 H. Lueken, in Magnetochemie, Teubner Verlag, Stuttgart, 1999.
- 57 K. S. Cole and R. H. Cole, J. Chem. Phys., 1941, 10, 98-105.
- 58 K. N. Shriyastava, Phys. Status Solidi B, 1983, 117, 437-458.
- 59 S. Sarwar, S. Sanz, J. van Leusen, G. S. Nichol, E. K. Brechin and P. Kögerler, Dalton Trans., 2020, 49, 16638-16642.